Extracellular alpha/beta-hydrolase from *Paenibacillus* species shares structural and functional homology to Tobacco Salicylic Acid Binding Protein 2

Rachael C. Wilkinson[a*1], Rahman Rahman Pour[b2], Shirin Jamshidi[c], Vilmos Fülöp[a] and Timothy D.H. Bugg[b*]

a) School of Life Sciences, University of Warwick, Coventry CV4 7AL, UK

b) Department of Chemistry, University of Warwick, Coventry CV4 7AL, UK

c) School of Cancer and Pharmaceutical Sciences, King's College London, SE1 9NH, UK

Corresponding authors:

Dr. Rachael C. Wilkinson, Sir William Dunn School of Pathology, University of Oxford, OX1 3RE. Email Rachael.wilkinson@path.ox.ac.uk.

Prof. Timothy D.H. Bugg, Department of Chemistry, University of Warwick, Coventry CV4 7AL, United Kingdom. Email T.D.Bugg@warwick.ac.uk.

Highlights:

- Identification of extracellular esterase from *Paenibacillus* species, PnbE.
- PnbE functions as an acetylesterase with optimum pH of 8.
- Crystal structure of PnbE shares structural homology to *N. tabacum* SABP2.
- Initial functional studies support PnbE functions as methyl salicylate esterase.

[1] Present Address: Sir William Dunn School of Pathology, University of Oxford, Oxford, OX1 3RE

[2] Present Address: Department of Bioengineering, University of Illinois at Urbana-Champaign, USA

Abstract

An alpha/ beta hydrolase annotated as a putative salicylate esterase within the genome of a species of *Paenibacillus* previously identified from differential and selective growth on Kraft lignin was structurally and functionally characterised. Feruloyl esterases are key to the degradation of lignin in several bacterial species and although this activity was investigated, no such activity was observed. The crystal structure of the *Paenibacillus* esterase, here denoted as PnbE, was determined at 1.32 Å resolution, showing high similarity to *Nicotiana tabacum* salicylic acid binding protein 2 from the protein database. Structural similarities between these two structures across the core domains and key catalytic residues were observed, with superposition of catalytic residues giving an RMSD of 0.5 Å across equivalent Cα atoms. Conversely, the cap domains of PnbE and *Nicotiana tabacum* SABP2 showed greater divergence with decreased flexibility in the PnbE cap structure. Activity of PnbE as a putative methyl salicylate esterase was supported with binding studies showing affinity for salicylic acid and functional studies showing methyl salicylate esterase activity. We hypothesise that this activity could enrich *Paenibacillus* sp. within the rhizosphere by increasing salicylic acid concentrations within the soil.

Keywords: alpha/beta-hydrolase; methyl salicylate esterase; Paenibacillus; rhizosphere; Salicylic Acid Binding Protein 2 (SABP2); salicylic acid

Database: structural data are available in the PDB under the accession number 6TJ2.

[3] List of Abbreviations: PnbE, Paenibacillus esterase; SABP, salicylic acid binding protein; Nt, Nicotiana tabacum; LB, Luria broth; PMSF, phenylmethylsulfonyl fluoride; PEG 3350, polyethylene glycol 3350; RMSD, root mean square deviation.

Introduction

Lignin, an aromatic heteropolymer, makes up 15-30% of plant cell wall lignocellulose found in plant biomass. The conversion of lignin into renewable chemicals as part of lignin-based biorefinery is a current area of scientific interest (Bugg and Rahmanpour, 2015; Zakzeski et al., 2010). Fungal degradation of lignin is well characterised throughout literature (Dashtban et al., 2010; Hatakka, 1994; ten Have and Teunissen, 2001), however, fungal enzymes are challenging to overexpress for industrial application. Bacterial breakdown of lignocellulose from plant biomass requires a range of different extracellular enzymes including Dyp-type peroxidases (Ahmad et al., 2011; Brown et al., 2012; Rahmanpour et al., 2016), multicopper oxidases (Granja-Travez et al., 2018; Majumdar et al., 2014), and in one case an extracellular manganese superoxide dismutase (Rashid et al., 2015). Multiple esterases have also been shown to be important for either the hydrolysis of ferulate-arabinose linkages within arabinoxylan (Millar et al., 2017; Topakas et al., 2007; Wong, 2006) or the hydrolysis of xylan acetyl groups (Degrassi et al., 1998; Kosugi et al., 2002; Shao and Wiegel, 1995; Till et al., 2013).

A wide variety of extracellular esterases have previously been implicated in the degradation of lignin (Frago et al., 2016; Hong et al., 2012; Millar et al., 2017; Raymer et al., 1990). Feruloyl esterases hydrolyse the ester linkages between ferulic acid and hemicellulose, with this activity important as straw lignins can contain up to 5% ferulic acid (Buranov and Mazza, 2008). Ferulic acid esterases have already been identified from *Aspergillus niger* (Faulds and Williamson, 1994; Record et al., 2003), *Pseudomonas fluorescens* (Bartolome et al., 1997) and *Streptomyces avermitilis* (Garcia et al., 1998).

Many bacterial species have already been shown to be involved in lignin degradation including *Ochrobactrum* sp. (Granja-Travez et al., 2018), *Sphingobacterium* sp. (Rashid et al., 2015), *Bacillus* sp. (Chandra et al., 2007; Degrassi et al., 1995), *Clostridrium* sp. (Rogers

et al., 1992; Wang et al., 2013) and *Paenibacillus* sp. (Mathews et al., 2016; Song et al., 2014). A *Paenibacillus* sp. was isolated from an environmental soil sample by selective and differential growth on Kraft lignin, with genome sequencing indicating similarity to the characterised *Paenibacillus* sp. FSL H7-0737 (Granja-Travez et al., 2018). A multicopper oxidase from this species was previously investigated as a putative polyphenol oxidase enzyme (Granja-Travez et al., 2018). Further investigation into other extracellular enzymes from this species is therefore required to identify how it is utilising Kraft lignin.

Bioinformatic analysis of the genome of this *Paenibacillus* species identified an extracellular esterase (NCBI Reference Sequence: WP_076283022), here denoted as PnbE, is described as a putative salicylate esterase. Esterases represent a diverse group of hydrolases capable of catalysing the cleavage and formation of ester bonds. The majority of esterases belong to the carboxyl esterase gene family within the α/β-hydrolase fold protein superfamily (Hotelier et al., 2004; Montella et al., 2012). A/β-hydrolase fold domains are found across a range of functionally diverse enzymes, with a plethora of different substrates. They share a conserved β-sheet core of five to eight strands joined by α-helices in an α/β/α sandwich format (Hotelier et al., 2004). PnbE shares 25% sequence homology with the methyl salicylate esterase (SABP2) from tobacco. Salicylic acid binding proteins (SABPs) were originally identified from protein extracts from tobacco leaves (Du and Klessig, 1997), with more recent studies using screening methods for identification (Manohar et al., 2014). Previously characterised salicylic acid binding proteins include carbonic anhydrases (SABP3 (Slaymaker et al., 2002)) and methyl salicylate esterases (SABP2 (Forouhar et al., 2005)). Methyl salicylate esterases catalyse the hydrolysis of the methyl group to form salicylic acid from methyl salicylate (Scheme 1). SABP2 has been implicated as important in both local and systemic resistance in plants (Kumar and Klessig, 2003; Tripathi et al., 2010). Enzymes catalysing release of

salicylic acid are of particular interest due to the prominence of salicylic acid in plant immunity (Durner et al., 1997) and root microbiome regulation (Lebeis et al., 2015).

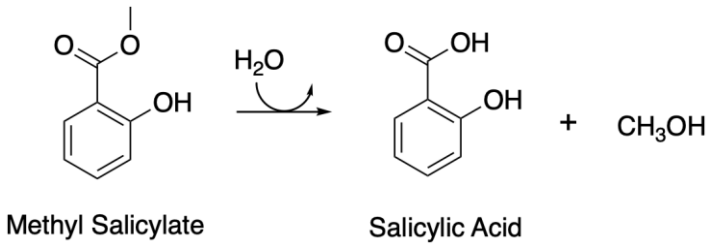

Scheme 1. Conversion of methyl salicylate to salicylic acid.

In order to explore the function of this esterase in more detail, we have expressed this enzyme, and we report the functional and structural characterisation of the recombinant enzyme. We show that PnbE shows activity as an acetylesterase with a range of *p*-nitrophenol esters and is functional as a methyl salicylate esterase but shows no activity as a feruloyl esterase. We describe the structural similarities and differences of PnbE and NtSABP2. This is the first structural deposition of a bacterial esterase shown to have methyl salicylate esterase activity.

Materials and Methods

Cloning of PNB esterase. Genomic DNA from *Paenibacillus sp*. was extracted using Wizard® Genomic DNA Purification Kit (Promega). Forward and reverse primers were designed for a truncated esterase gene without the signal peptide to improve the expression. The forward primer (5′ CACCGCC GCT AAC CAC AAA TCC TCT ACC AAA CAG3′) and reverse primer (5′ CTA ATC TCT ACC CGC CTT GAC CAT C 3′) were designed for PCR amplification using Platinum Pfx-DNA polymerase (Invitrogen) as per manufacturer's instructions. The amplified gene was cloned using the Champion™ pET 151 Directional TOPO® Expression Kit (Invitrogen) into expression vector pET151 and transformed into *E. coli* TOP10 competent cells (Invitrogen). Purified plasmid (pET151::PnbE) was sequenced to confirm ligation and accuracy of the sequence.

Expression and Purification. Recombinant hexa-histidine tagged *Paenibacillus* esterase (PnbE) was expressed in *E. coli* BL21 cells (Invitrogen). To 2 L LB broth containing 100 μg/mL ampicillin a 1% inoculum of overnight starter culture of *E. coli* BL21 cells containing pET151::PnbE was added. The culture was then incubated at 37 °C, 180 rpm until an OD_{600} of 0.6 was reached. Expression was induced by the addition of 0.5 mM IPTG followed by incubation at 15 °C overnight. Cells were harvested by centrifugation at 4000 ×g at 4 °C for 20 minutes. PnbE was purified using Nickel affinity chromatography. Harvested cells were resuspended in 20 mL lysis buffer (50 mM sodium phosphate pH 8.0, 300 mM NaCl, 1 mM PMSF). Cells were lysed with a constant system cell disrupter and debris pelleted by centrifugation at 10,000 ×g at 4 °C for 30 minutes. Cleared lysate was then loaded onto a Ni-NTA column (HisTrap HP, 1 mL) which had been pre-equilibrated in wash buffer (50 mM sodium phosphate pH 8, 300 mM NaCl, 20 mM Imidazole). The column was then washed with 100 mL of wash buffer before the protein was eluted at 0.5 ml/min with elution buffer

(50 mM sodium phosphate pH 8.0, 300 mM NaCl, 250 mM imidazole). PnbE was further purified using size exclusion chromatography with a Sephadex G-75 column (Sigma-Aldrich, St Louis, MO, USA). The column was equilibrated in 50 mM sodium phosphate pH 7.4, 100 mM NaCl at 0.75 mL/min.

PnbE Activity with Esters. PnbE activity assays with *p*-Nitrophenyl ester substrates (*p*-nitrophenyl benzoate, *p*-nitrophenyl palmitate, *p*-nitrophenyl phosphate, *p*-nitrophenyl acetate, *p*-nitrophenyl octanoate) were set up in duplicate in 50 mM sodium phosphate pH 8.0, 300 mM NaCl with 6 μM PnbE and 2mM of the substrate. Reactions were monitored at 25 °C by a Cary 50 spectrophotometer by the appearance of *p*-nitrophenol at 405 nm (ε 18,000 M^{-1} cm^{-1}) over time.

PnbE pH-rate Profile. The pH-rate profile for PnbE was determined at 25 °C using the assay described previously with *p*-nitrophenyl acetate (1 mM) as the substrate over a range of pH buffers. The buffers used contained 50 mM boric acid, 50 mM sodium acetate and 50 mM potassium phosphate and were then adjusted to the desired pH (every 0.5 unit between 3.5 and 10.5).

Analytical Size Exclusion Chromatography. A Superose 6 column (10 mm × 300 mm, GE Healthcare) was used to estimate the apparent molecular mass of purified PnbE (~ 1 mg/mL). Protein samples were applied (1 mL/min) to a pre-equilibrated column in 50 mM sodium phosphate pH 7.4, 150 mM NaCl. Apoferritin (443 kDa), β-amylase (200 kDa), alcohol dehydrogenase (150 kDa), bovine serum albumin (66 kDa) and carbonic anhydrase (29 kDa) were used as protein standards for calibration of the column. Elution of the protein samples were monitored by absorbance at 280 nm.

Binding of PnbE to Salicylic Acid. Binding of salicylic acid to PnbE was determined using thermal shift assays. Reactions with 5× Sypro Orange, 10 μM of PnbE and salicylic acid (at final concentrations of 0 to 4 mM) were made up in 10 mM NaH_2PO_4, 50 mM NaCl pH 8 in

a 96-well low profile white skirted plate (ThermoFisher). The plates were sealed with sealing films (EXCEL Scientific) and heated in an Agilent Technologies Stratagene MX300 5P Real Time PCR Detection System from 25 to 100 °C in increments of 0.1 °C. Fluorescence changes in the wells of the plate were monitored with the wavelengths for excitation and emission at 490 nm and 575 nm respectively. Binding curve was calculated using the single site ligand binding equation described by Vivoli *et al.* (Vivoli et al., 2014).

PnbE Salicylate Esterase Activity. Reaction contained 0.2 mg/mL PnbE and 10 mM methyl salicylate and were incubated at room temperature for 30 minutes. The reaction was stopped by incubating at 100 °C for 5 minutes. The reaction was then analysed by HPLC using Phenomenex Luna 5 μm C18 reverse phase column (100 Å, 50 mm, 4.6 mm) on a Hewlett–Packard Series 1100 analyser, at a flow rate of 0.5 ml/min, with monitoring at 210 nm. The gradient was as follows: 10 to 30% MeOH/H_2O over 10 min, 30 to 40% MeOH/H_2O from 10 to 20 min, 40 to 70% MeOH/H_2O from 20 to 30 min and 70 to 100% MeOH/H_2O from 30 to 40 mi. Peaks corresponding to methyl salicylate or salicylic acid were identified by HPLC analysis of known standards (Fig. A.1).

Crystallization, data collection, and structure determination. Pure recombinant PnbE (21 mg/mL) in 50 mM sodium phosphate buffer pH 7.4, 150 mM NaCl was subjected to crystallisation screening using a Mosquito liquid handling robot (TTP Labtech). Protein (200 nL) was mixed with 200 nL of crystallisation solution from commercially available screens in MRC 96-well 2-drop crystallisation plates (Molecular Dimensions). Plates were sealed with sealing films (EXCEL Scientific) and incubated at 22 °C. Crystals appeared in a number of conditions between 1-2 weeks. Rod shaped crystals were grown in condition E1 of the PactPremier crystallisation screen (Molecular Dimensions) containing 0.2 M sodium fluoride, 20% PEG 3350. Crystals were removed from drops using a mounted Litholoop (Molecular Dimensions), cryoprotected in crystallisation solution containing 20% ethylene glycol, and

flash-frozen in liquid nitrogen. X-ray diffraction data to a resolution of 1.32 Å were collected at 100K at the beam line I03 at the Diamond Light Source, U.K. using a Pilatus 6M detector. All data were indexed, integrated and scaled using the XDS package (Kabsch, 2010). Further data handling was carried out using the CCP4 software package (Dodson et al., 1997). The structure was solved by molecular replacement using the automated pipeline by BALBES (Long et al., 2008), with the primary search model as PDB: 3DQZ. The structure was further refined by alternate cycles of manual refitting using Coot (Emsley and Cowtan, 2004) and Refmac (Murshudov et al., 1997). Water molecules were added to the atomic model automatically using ARP (Langer et al., 2008), at the positions of large positive peaks in the difference electron density, only at places where the resulting water molecule fell into an appropriate hydrogen bonding environment. Restrained isotropic temperature factor refinements were carried out for each individual atom with overall anisotropic scaling. Data collection and refinement statistics are given in Table 1.

Molecular Dynamics and Molecular Docking. The protein structure of PnbE (6TJ2) determined by x-ray crystallography was used for computational study. Missing N-terminal amino acids were input based on the known sequence of the protein using Accelrys discovery studio. After minimising and equilibrating the structure, 10 ns conventional molecular dynamics (cMD) simulations followed by 500 ns accelerated molecular dynamics (aMD) simulations were done using AMBER 16 package program (Case et al., 2005). MD analysis was used to extract the top 10 dominant conformation structures for running molecular docking. AutoDock SMINA (Koes et al., 2013) was used for blind docking of methyl salicylate and salicylic acid to determine the most probable binding site. GOLD (Jones et al., 1997, 1995) molecular docking was then used to determine the best-docked pose for each system, based on low binding energy and related score (Table A3.). Molecular dynamic

simulations, as described previously, for SABP2 (PDB:1Y7I) was also completed for determination of flexibility and fluctuations for comparison with PnbE.

Accession Number. The co-ordinates and structure factors of the characterised *Paenibacillus* sp. esterase has been deposited in the PDB with the accession code 6TJ2.

Results

Identification and Purification of *Paenibacillus* Esterase (PnbE). *Paenibacillus* sp. was isolated from a soil sample collected from Hampton Lucy, Warwickshire and differentially grown on Kraft lignin and minimal media (Granja-Travez et al., 2018; Rashid et al., 2017). The genome was sequenced and explored esterase enzymes, with preference for those exported from the cell. The gene for PnbE from *Paenibacillus* sp. was chosen for further exploration as a putative extracellular esterase. The sequence for PnbE is currently identified as an α/β-hydrolase by BLAST with the sequence ID of WP_076283022.

To improve overexpression of PnbE the sequence encoding the signal peptide was excluded by designing primers for PCR amplification of the gene without the signal peptide. Boundaries for the signal peptide were identified using SignalP-5.0 server (Nielsen et al., 1997) (Fig. A.2). The gene for PnbE was amplified from *Paenibacillus* 351 genomic DNA and cloned into a pET vector. The encoded protein is 253 amino acids in length (28.3 kDa) in the absence of the signal peptide. Expression in *E. coli* BL21 yielded high levels of PnbE (35 mg/L cell culture) which was then purified using metal affinity chromatography (Fig. A.3) and further purified by size exclusion chromatography.

Structure determination. The crystal structure of PnbE has been determined at 1.32 Å resolution (PDB accession 6TJ2). The asymmetric unit of the crystal contained three molecules with the space group $P2_12_12_1$ (Fig. 1a). The current atomic model contains residues 11-253 for the three chains within the asymmetric unit. Structural analysis shows a core domain with typical α/β-hydrolase fold and an α-helical cap domain (Fig. 1b).

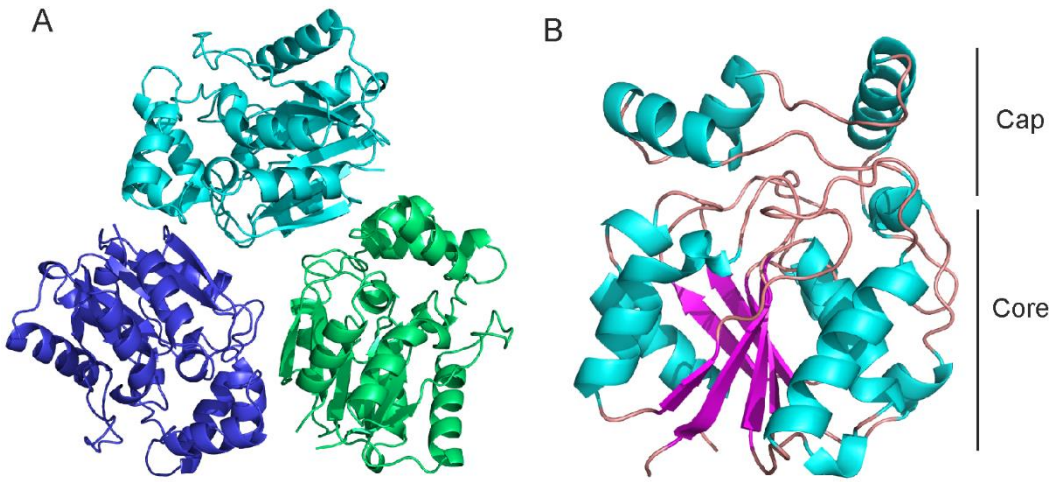

Figure 1. Overall structure of PnbE. A. Three chains present in the asymmetric unit. B. Subunit of PnbE, coloured by secondary structure (β-strands: magenta, α-helices: turquoise, loops: pale pink), with core and cap domains denoted.

Overall Structure. Three chains are observed within the asymmetric unit but PISA analysis (Krissinel and Henrick, 2007) suggested the absence of any meaningful interfaces between the subunits (Complex Formation Significance Scores of 0.000 between chains) (Table A.2). To further investigate this analytical size exclusion chromatography was used to confirm the multimeric state of the purified protein. PnbE formed one major peak with an apparent mass of ~150 kDa which suggests a hexamer (6 × 28.3 kDa, 170 kDa) (Fig. 2). Crystal structures for other α/β-hydrolase have also contained multiple chains within the asymmetric unit but have been shown to be active in the monomeric form (Forouhar et al., 2005; van Pouderoyen et al., 2001). We hypothesise that during purification and crystallisation the protein is at an unnaturally high concentration and therefore forms a multimeric structure of trimer or hexamer. Despite the presence of 10 hydrogen bonds and 3 salt bridges between non-crystallographic trimeric subunits within the ASU, PISA analysis (Krissinel and Henrick,

2007) concluded these did not have a role in complex formation but instead were a result of crystal packing. We therefore suggest that the active enzyme is monomeric.

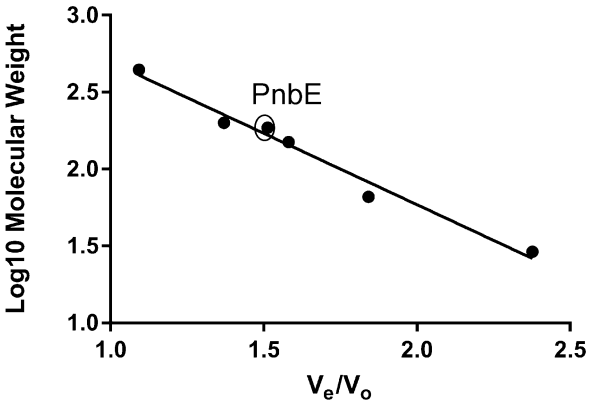

Figure 2. Multimeric state of PnbE established using analytical gel filtration. Position of PnbE with relation to standards (Apoferritin (443 kDa), β-amylase (200 kDa), alcohol dehydrogenase (150 kDa), bovine serum albumin (66 kDa) and carbonic anhydrase (29 kDa)).

Each subunit divides into two domains, a core domain (residues 11-115, 182-253) and a cap domain (residues 116-181) (Fig. 1b). The core domain contains six stranded β-sheet surrounded by eight α-helices, which fits the canonical structure of an α/β-hydrolases (Holmquist, 2000; Hotelier et al., 2004; Nardini and Dijkstra, 1999). The cap domain is made up of five α-helices.

Table 1. Crystallography data collection and refinement statistics.

Data collection[a]	
Space group	$P2_12_12_1$
Cell dimensions [*a*, *b*, *c* (Å)]	47.86, 112.43, 126.85
Wavelength (Å)	0. 91587
Resolution (Å)	57-1.32 (1.39-1.32)
Observations	1039504 (135229)
Unique reflections	159905 (10462)
R_{sym}	0.059 (0.739)
I/σ (I)	17.7 (2.0)
Completeness (%)	99.2 (94.7)
Redundancy	6.5 (6.1)
$CC_{1/2}$	0.999 (0.737)
Refinement	
R_{cryst}	0.161 (0.289)
Reflections used	153475 (10113)
R_{free}	0.183 (0.296)
Reflections used	6430 (449)
Non-hydrogen atoms	6444 (667 water molecules)
B-factor (Å^2)	
Protein	16.7
Water	27.3
Root-mean-squared deviation	
Bond lengths (Å)	0.015
Bond angles (°)	1.9
DPI coordinate error (Å)	0.048

[a]Values in parentheses are for highest-resolution shell.

Structural Homology to SABP2. A sequence-based search within the protein database (PDB) showed highest similarity of PnbE to the *N. tabacum* salicylic acid binding protein (NtSABP2) (PDB: 1XKL) with 26% identity and 41% positives. This was supported by structural comparison using DALI (Holm, 2020) which showed highest similarity with a z-score of 26.1 for a hydroxynitrile lyase (PDB: 3DQZ) and a z-score of 25.3 for NtSABP2 (PDB: 1Y7I), with z-scores over three indicative of some structural similarity.

Superposition of NtSABP2 (PDB: 1XKL) and PnbE using SuperPose (Krissinel and Henrick, 2004) gave a local RMSD of 1.63 Å over Cα atoms within residues 3-48 (PnbE) and 11-56

(NtSABP2) (Fig. 4a). Superposition of PnbE with a hydroxynitrile lyase (HNL) from Arabidopsis thaliana (3DQZ) yielded a slightly higher local RMSD of 1.07 Å over Cα atoms within residues 3-46 (3DQZ) and 11-54 (PnbE) but a far worse global RMSD (of 9.38 Å vs 6.5 Å respectively). In addition, PnbE was found to contain a glycine (Gly20) and methionine (Met233) at corresponding positions of the threonine and lysine required for HNL activity (Padhi et al., 2010). Further analysis was therefore focussed on NtSABP2.

The core domains of PnbE and NtSABP2 share a high level of similarity with both containing six β-strands surrounded by eight α-helices (Fig. 3a). Despite the average number of residues in an α-helix is ~10 residues (Kumar and Bansal, 1998), of the eight α-helices in the core domain within PnbE three are 1-turn α-helices (average of 4 residues) whereas in NtSABP2 only two are 1 turn α-helices.

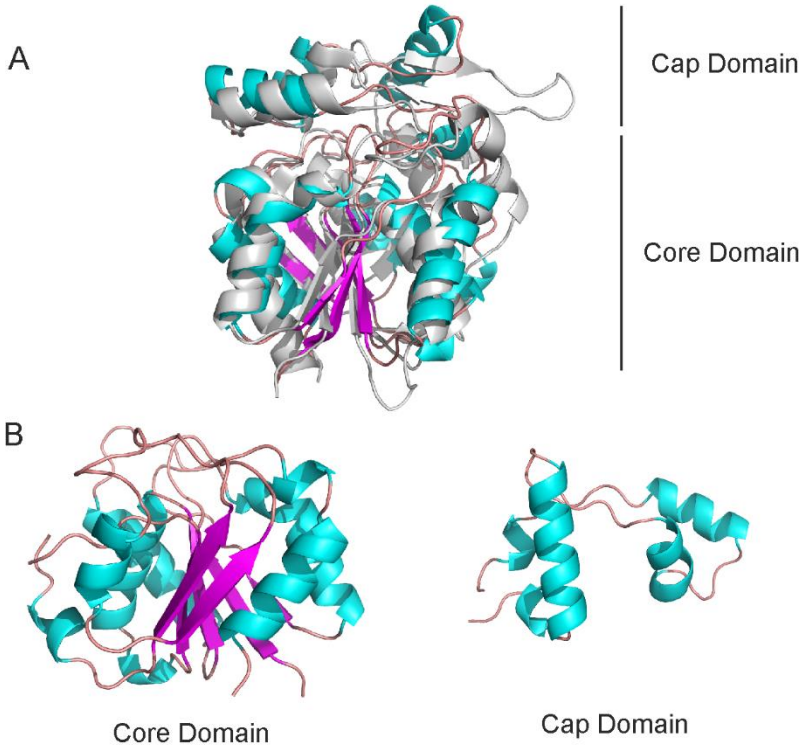

Figure 3. Structural similarities between PnbE and NtSABP2. A. Structural superposition of cartoon representations of PnbE and NtSABP2. B. Cartoon representation of core domain and cap domain for PnbE. PnbE coloured by secondary structure elements (β-strands: magenta, α-helices: turquoise, loops: pale pink) and NtSABP2 coloured grey.

The cap domains show greater divergence between NtSABP2 and PnbE. In NtSABP2 the cap domain is shown to contain three α-helices and two β-strands covering around 70 residues (Forouhar et al., 2005). Conversely, in PnbE there are five α-helices and no β-strands covering 67 residues (Fig. 3b). Within the cap domain there are two 1-turn α-helices at the hinge region of the cap domain as well as three that overlay well with those from NtSABP2 (Fig. 3a). Interestingly, RMSF plots indicate that the cap domain within PnbE (residues 116-181) shows reduced flexibility when compared to that within NtSABP2, with PnbE conversely showing greatest flexibility within the core domain (Fig. 4). Three flexible regions within the PnbE core domain were observed (Fig. 4b) with flexible region two containing the

residue Glu46, the oxyanion zone II residue which is essential for the stable formation of the oxyanion hole (Dimitriou et al., 2019). Furthermore, flexible region four contains the catalytic acid, Asp202, from the catalytic triad.

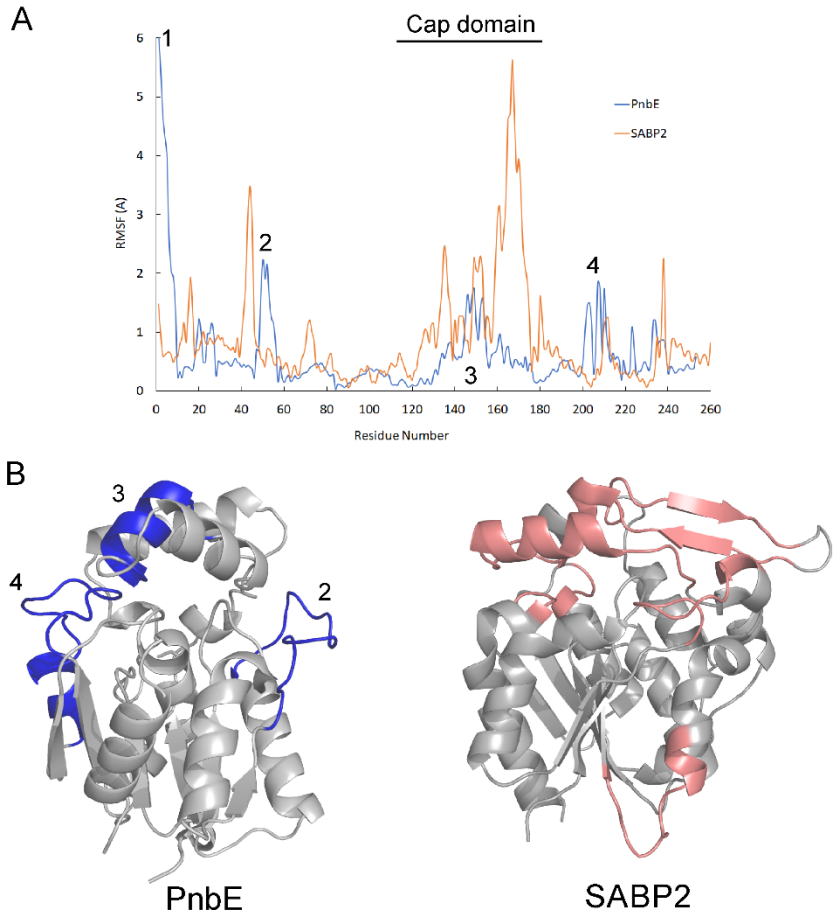

Figure 4. Predicted structural flexibility for PnbE and NtSABP2. A. Root Mean Square fluctuation (RMSF) plots for PnbE (6TJ2) and NtSABP2 (1XKL). B. Cartoon representation PnbE and NtSABP2 coloured grey, with flexible regions highlighted in blue and pink respectively. Flexible regions are numbered according the graph in 4a.

CAVER analysis (Stourac et al., 2019) of both apo structures supports this with seven putative tunnels observed for NtSABP2 and only five putative tunnels observed for PnbE originating from the cavity around the active site. Comparison of the top throughput tunnel

for each structure shows an increase in length of the tunnel by ~1.5× and width of the tunnel bottleneck by ~1.3× comparatively between NtSABP2 and PnbE (Fig. A.4, Table A.3.).

Active Site. The majority of α/β-hydrolase contain a catalytic triad composed of a Nucleophile-His-Acid (Holmquist, 2000). In NtSABP2 these residues are Ser81, Asp210 and His238 (Forouhar et al., 2005) and from sequence and structural alignment comparable residues in PnbE are Ser85, Asp202 and His232. The catalytic triad residues are all situated in loops at the top of the core domain, with the putative active site enclosed by the cap domain (Fig. 5a).

PnbE appears to belong to group I (+++++) of the α/β-hydrolases classifications, as described by Dimitriou *et al*. in 2019 (Dimitriou et al., 2019). Other members of this group include SABP2, whereas AtHNL and HbHNL belonging to groups II and IV respectively. Comparison of the five key catalytic residues for PnbE, SABP2 and hydroxynitrile lyases are detailed in Table 2.

Table 2. Six key residues of the catalytic site surrounding the catalytic nucleophile.

	PnbE (PDB:6TJ2)	**SABP2 (PDB:1XKL)**	**AtHNL (PDB:3DQZ)**	**HbHNL (PDB:3C6X)**
$X_{oxyII-2}$	His19	His11	His11	His10
$X_{oxyII-1}$	Gly20	Gly12	Asn12	Thr11
W/Y/F	Trp28	Trp20	Trp20	Trp19
X_{ozII}	Glu46	Asp38	Glu38	Asp37
X_{nuc-1}	His84	His80	Phe80	Glu79
XIV	Asp109	Ala105	Asn105	Asn104

PnbE and NtSABP2 show strong conservation in the G-X-S-X-G motif, with both containing histidine at the nucleophile -1 position (X_{nuc-1}). Key residues involved in the formation and stabilisation of the oxyanion hole appear to be conserved between NtSABP2 and PnbE (Fig. 5b), including the oxyanion II -1 and -2 residues ($X_{oxyII-1}$/$X_{oxyII\ -2}$) and the tryptophan residue within the aromatic dipeptide located beneath the nucleophile and oxyanion hole (W/Y/F). The remaining aromatic residue in the aromatic dipeptide, however, differs between the two structures in both residue and position. The acidic residues at the oxyanion zone II position (X_{ozII}) also varies between the two structures, with glutamate and aspartate for PnbE and NtSABP2 respectively (Fig. 5b).

A/β-hydrolases can be further characterised by the positioning of the catalytic acid residue either at the end of strand β7 (Group A) or β6 (Group B) (Dimitriou et al., 2017). The co-ordinating position IV residue (XIV) located immediately after the strand β6 aids the co-ordination of the catalytic histidine loop above the plane of the catalytic acid zone (Dimitriou et al., 2017). Within PnbE the residue at position IV is Asp109, this is divergent from both NtSABP2 with the small non-polar residue Ala105 at this position and from AtHNL and HbHNL which contain Asn (Asn105 and Asn104 respectively). The presence of an acidic residue at this position is unusual and could implicate the formation of a structural catalytic tetrad, with both Asp109 and the catalytic acid Asp202 interacting with the catalytic histidine His85, rather than the classical catalytic triad previously observed for similar enzymes.

Superposition of the salicylic acid from NtSABP2 into the active site of PnbE shows close proximity to the catalytic triad residues, with around 3 Å distance from either His232 or Ser85 respective hydroxyl groups to SA comparable with distances observed for NtSABP2 (Fig. 5a). Positioning of the residues are very similar between the structures between the salicylic acid bound NtSABP2 (PDB:1Y7I) and the apo form of PnbE. Forouhar *et al.* previously showed that there was minimal difference observed between the ligand bound

(PDB:1Y7I) and apo form of NtSABP2 (PDB: 1XKL), with an RMSD of 0.45 Å between equivalent Cα atoms (Forouhar et al., 2005). Superposition of the catalytic residues between PnbE and NtSABP2 show a high level of similarity with an RMSD 0.50 Å between equivalent Cα atoms.

To further explore the potential active site blind molecular docking was used to determine the putative binding site, with ligands consistently occupying the pocket within the protein containing the catalytic triad residues (Ser85, His232 and Asp202). Flexible molecular docking of methyl salicylate (MSA) and salicylic acid (SA) using GOLD (Jones et al., 1997, 1995) in the SMINA-located binding site yielded good scores and energies of bindings for all PnbE conformers tested (Table A.1). Figure 5c shows the 2D and 3D structure of best scored docking of SA with a binding energy of -25.4 kcal/mol for SA and -24.43 kcal/mol for MSA. Key residues found to bind SA include Asp109, Phe111, Phe212 and Ser85 (Fig. 5c) whereas those for binding MSA include Ile205, Leu149, Phe111, Phe212 and Thr153 (Figure A.5).

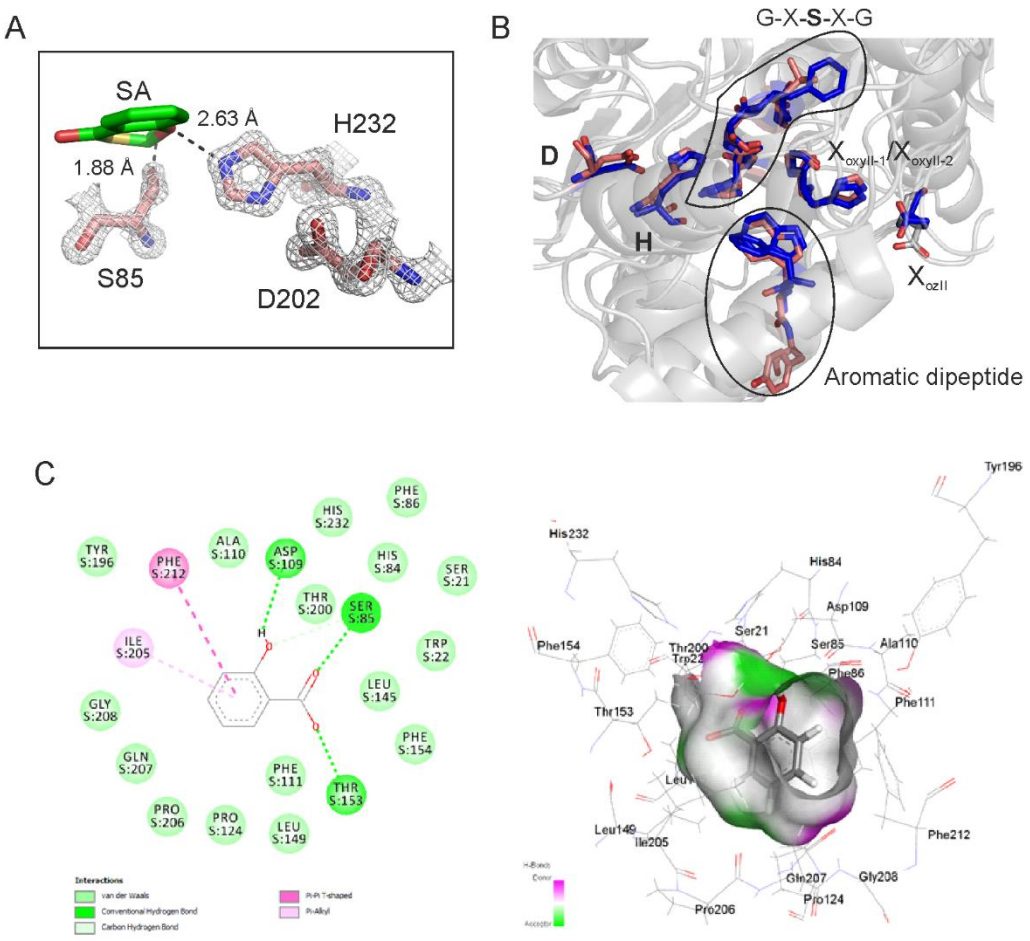

Figure 5. Putative Active Site for PnbE and similarity to NtSABP2. A. Superimposed SA in PnbE active site with catalytic triad residues displayed as pale pink sticks with electron density (σ level 2) shown and superposition of SA (displayed as green stick model) from NtSABP2 structure. B. superposition of key residues in PnbE active site (displayed as blue stick models) and corresponding residues in NtSABP2 (displayed as pale pink stick models), with catalytic triad residues are highlighted in bold. C. 2D and 3D structures of docked SA into the active site of PnbE. Key residues in ligand binding and the binding pocket are represented on the left and right respectively.

Esterase Activity. As PnbE is a previously uncharacterised esterase activity was originally tested with a range of different *p*-nitrophenol esters. PnbE was found to be active with *p*-nitrophenyl acetate (0.70 specific activity) and *p*-nitrophenyl octanoate (0.17 specific

activity) but showed no activity with *p*-nitrophenyl benzoate, *p*-nitrophenyl palmitate or *p*-nitrophenyl phosphate as a substrate (Fig. 6a). A pH-rate profile for PnbE with *p*-nitrophenyl acetate as a substrate showed the optimal pH for activity was pH 8.0 (Fig. 6b). Steady state kinetic parameters for PnbE with *p*-nitrophenyl acetate were calculated using a series of reaction time courses over a range of substrate concentrations (Fig. 6c). Analysis of reaction rates (V_0) vs. substrate concentration gave a calculated K_M of 627 ± 53 μM. These data suggest that the enzyme can function as an acetylesterase with activity levels similar to those seen for previously characterised acetylesterases (Millar et al., 2017; Watanabe et al., 2015).

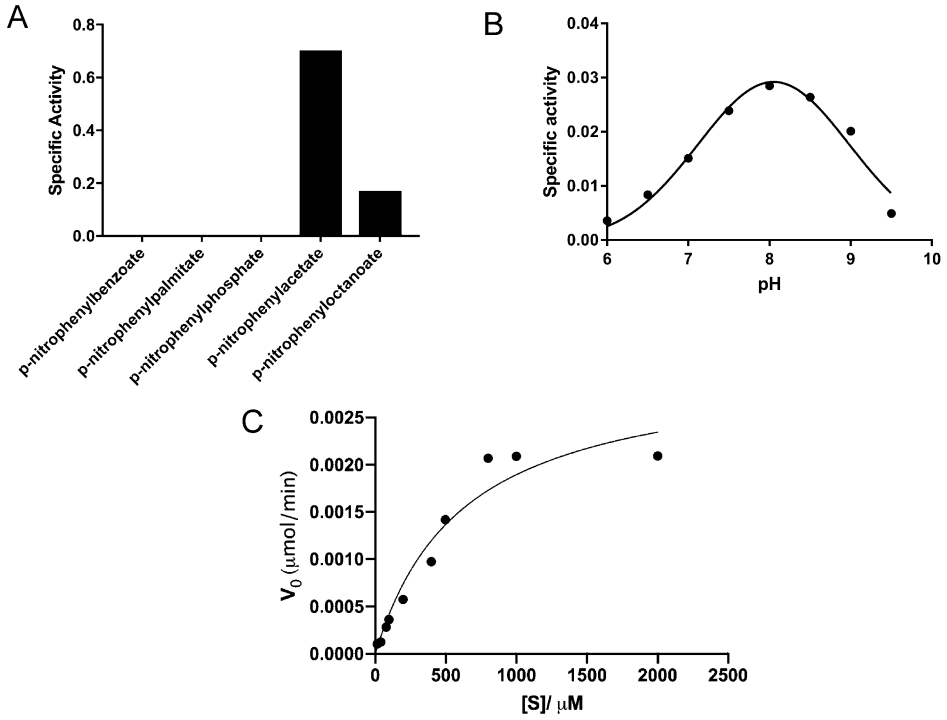

Figure 7. Esterase activity of PnbE. A. Specific esterase activity for PnbE in the presence of a range of putative substrates. B. pH profile for PnbE activity with *p*-nitrophenyl acetate. C. Michaelis-Menten plot for PnbE with 4-nitrophenyl acetate as a substrate.

Binding of salicylic acid (SA) to PnbE was determined using thermal shift assays (Huynh and Partch, 2015). The melting curves for PnbE shifted to the right with increasing concentration

of SA (Fig. 7a). The calculated melting temperature (Tm) for PnbE increased with the concentration of salicylic acid (Fig. 7b), confirming the ability of PnbE to bind SA.

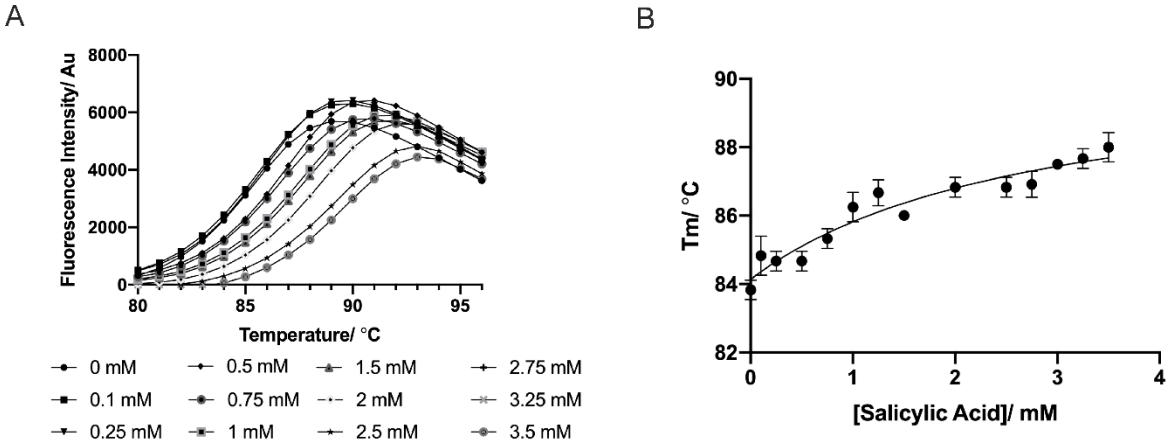

Figure 8. Binding affinity of PnbE for salicylic acid. A. Melting curves for PnbE with increasing concentrations of SA using thermal shift assays. B. SA binding curve for PnbE based on calculated melting temperatures (Tm) for PnbE over a range of SA concentrations.

With NtSABP2 detailed as a methyl salicylate esterase, the ability of PnbE to catalyse the hydrolysis of methyl salicylate to form salicylic acid was confirmed using HPLC analysis (Fig. 7b). Incubation of PnbE with methyl salicylate showed conversion to salicylic acid when compared to known standards, demonstrating that PnbE can function as a methyl salicylate esterase with a calculated k_{cat} of 0.40 s^{-1}. This can be compared to NtSABP2 which has a reported k_{cat} value of 0.45 s^{-1} (Forouhar et al., 2005).

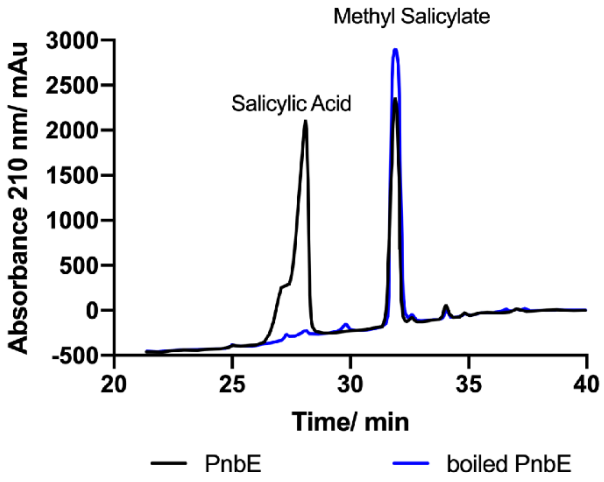

Figure 7. HPLC trace for the conversion of methyl salicylate to salicylic acid by 200 µg PnbE (black line) in a 30 min assay (see Materials and Methods) compared to inactive (boiled) PnbE (blue line).

Discussion

Paenibacillus species can be found in both bulk soil (Uhlik et al., 2009) and the rhizosphere (Rosado et al., 1998; Timmusk et al., 2009) and have been identified as important in the degradation of lignin (Chandra et al., 2007). With limited information on the classes of extracellular enzymes involved in lignin degradation by *Paenibacillus* species we aimed to characterise the structure and function of PnbE, annotated as a salicylate esterase. We have verified activity as a methyl salicylate esterase, though PnbE shows no feruloyl esterase activity.

Sequence analysis of PnbE showed homology with *Nicotiana tabacum* Salicylic Acid Binding Protein 2 (NtSABP2), a methyl salicylate esterase. SABP2 enzymes have been shown to be important in local and systemic acquired resistance in plants (Kumar and Klessig, 2003; Tripathi et al., 2010). The phytohormone salicylic acid and derivatives are well known to be integral to plant immunity (Durner et al., 1997), with roles in cell response to infection as well as protection (Dieryckx et al., 2015; Kim et al., 2017).

Here we have described the determination of the structure of PnbE to 1.32 Å resolution which can be classed as a group I α/β-hydrolase, according to the definitions by Dimitriou *et al.* (Dimitriou et al., 2019). Structural analysis using DALI (Holm, 2020) showed highest similarity of the structure to that of a hydroxynitrile lyase (PDB:3DQZ) with a z-score of 26.1 and NtSABP2 (PDB:1Y7I) with a z-score of 25.3. Hydroxynitrile lyases (HNLs) and esterases differ mechanistically and yet share key structural components such as the catalytic triad (His-acid-nucleophile) and oxyanion hole (Rauwerdink and Kazlauskas, 2015). There are however structural variances between the two, with HNLs containing a threonine which blocks the entrance to the oxyanion hole via its side chain and a lysine within the active site that can hydrogen bond with cyanide (Padhi et al., 2010; Rauwerdink and Kazlauskas, 2015). Mutations in these two residues has been shown to significantly reduce HNL activity in *Hevea brasiliensis* HNL. Furthermore, esterase activity and HNL activity are antagonistic and two mutations in NtSABP2 (Gly12Thr and Met239Lys) were sufficient to greatly reduce esterase activity whilst introducing HNL activity (Padhi et al., 2010). Structural analysis of PnbE shows that it does not contain either of the residues linked to HNL activity, with glycine and methionine at the corresponding positions respectively (Gly20 and Met233). Other differences include that PnbE and HNL belong to different α/β hydrolase groups (I and IV respectively). Therefore, despite marginally closer structural similarity to a hydroxynitrile lyase, PnbE is unlikely to function as one. Conversely, PnbE shares several similarities with NtSABP2 regarding key residues involved in the formation and stabilisation of the oxyanion hole and catalytic activity, with catalytic triad residues superimposing with an RMSD of 0.498 Å between equivalent Cα atoms. Regardless of the high levels of consensus between the structures it is worth noting that sequence alignment showed that PnbE still aligns more closely to other bacterial esterases than plant equivocal used for structural comparisons (Fig. A.6).

Despite structural similarities between PnbE and NtSABP2 there are differences in their substrate specificities, with lipase activity for *p*-nitrophenyl palmitate observed in NtSABP2 (Forouhar et al., 2005) but not in PnbE. Structural comparison using molecular dynamic simulations showed different flexibility profiles, which could perhaps be unexpected as proteins within the same fold families have been noted previously to have similar flexibility profiles (Benson and Daggett, 2012). The reduced flexibility observed in the cap domain of PnbE is corroborated by CAVER analysis (Stourac et al., 2019) showing fewer predicted tunnels from the active site. Furthermore, the top throughput tunnel for PnbE is shorter and narrower than that from NtSABP2. These data suggest that the active site in PnbE is less accessible and this may explain the more stringent substrate specificity observed, particularly for bulkier substrates such as *p*-nitrophenyl benzoate. The cap domains of α/β-hydrolases are also known to contribute important residues to the active site (Rauwerdink and Kazlauskas, 2015), for PnbE there are two residues within the cap domain predicted to be involved in binding SA or MSA, Leu149 and Thr153. Both of these residues are located within the only area of increased flexibility within the cap domain of PnbE, suggesting that the conformation of the cap domain is important in the binding of these compounds. Lipase activity is dependent on seclusion of the active site from solvent (Bornscheuer, 2002) and five residues from the cap domain were highlighted as shielding for SA in the active site of NtSABP2: Asn123, Trp131, Phe136, Met149 and Leu181 (Forouhar et al., 2005). Comparative shielding is not observed in PnbE (Fig. A.7.) and consequently this could account for the absence of lipase activity in PnbE.

Confirmation of PnbE as a methyl salicylate esterase, originally based on sequence and structural homology, using biochemical techniques showed binding of salicylic acid to PnbE and conversion of methyl salicylate to salicylic acid. We therefore propose that PnbE serves as a multi-functional extracellular esterase with acetyl esterase activity but more interestingly

catalytic activity for the conversion of methyl salicylate to salicylic acid with a calculated k_{cat} of 0.4 s-1. Methyl salicylate esterases have been described previously from Tobacco (Forouhar et al., 2005), Arabidopsis (Vlot et al., 2008) and Popular (Zhao et al., 2009) species but there seems to be limited information for homologous activity within bacterial enzymes and here we describe, to our knowledge, the first structure of a bacterial methyl salicylate esterase.

The genera *Paenibacillus* is a member of the phylum Firmicutes, which have been previously found within the rhizosphere (Mendes et al., 2013). Despite being isolated in both bulk soil and rhizosphere, a recent study showed depleted levels of Firmicutes in bulk soil compared to those in the rhizosphere for *Populus* species in Clatskanie soil (Veach et al., 2019). Increased salicylic acid concentration within the rhizosphere modulates the microbiome with an observed increase the prevalence of Firmicutes and Actinobacteria species whilst decreased prevalence of Bacteroidetes and Acidobacteria species (Lebeis et al., 2015). As a member of the Firmicutes, *Paenibacillus* species, could be predicted to be at higher concentrations within the rhizosphere and we propose that having an extracellular esterase capable of releasing salicylic acid from methyl salicylate would therefore be beneficial. The means to manipulate salicylic acid concentrations within the rhizosphere could allow for enrichment of *Paenibacillus* species and other Firmicutes whilst reducing competition by depleting Bacteroidetes and Acidobacteria species. We hypothesise this would likely be soil or plant specific, as Veach *et al*. conversely found a positive correlation between salicylic acid and the acidobacterial Koribacteraceae and Solibacteria whilst describing no positive correlation with Firmicutes for *Populus*-associated microbiomes (Veach et al., 2019).

Conclusion

PnbE, an extracellular esterase from a *Paenibacillus* species differentially and selectively grown on Kraft lignin, shares structural similarities with the methyl salicylate esterase SABP2 from *Nicotiana tabacum*. This observation is compounded by functional studies which show binding of salicylic acid and catalytic turnover of methyl salicylate to salicylic acid. These data suggest a possible alternative function for PnbE to promote salicylic acid concentrations in the rhizosphere of plants which in turn could lead to enrichment of *Paenibacillus* species within the root microbiome.

Acknowledgements. We would like to acknowledge Diamond Light Source and the support of beamline scientist Dr Katherine McAuley in the collection of X-ray diffraction data.

Funding. This work was supported by the Biotechnology and Biological Sciences Research Council (BBSRC) grants BB/M003523/1 and BB/M025772/1.

References

Ahmad, M., Roberts, J.N., Hardiman, E.M., Singh, R., Eltis, L.D., Bugg, T.D., 2011. Identification of DypB from Rhodococcus jostii RHA1 as a lignin peroxidase. Biochemistry 50, 5096–5107. https://doi.org/10.1021/bi101892z

Bartolome, B., Faulds, C.B., Kroon, P.A., Waldron, K., Gilbert, H.J., Hazlewood, G., Williamson, G., 1997. An Aspergillus niger esterase (ferulic acid esterase III) and a recombinant Pseudomonas fluorescens subsp. cellulosa esterase (Xy1D) release a 5-5' ferulic dehydrodimer (diferulic acid) from barley and wheat cell walls. Appl Env. Microbiol 63, 208–212.

Benson, N.C., Daggett, V., 2012. A Comparison of Multiscale Methods for the Analysis of Molecular Dynamics Simulations. J. Phys. Chem. B 116, 8722–8731. https://doi.org/10.1021/jp302103t

Bornscheuer, U.T., 2002. Microbial carboxyl esterases: classification, properties and application in biocatalysis. FEMS Microbiol. Rev. 26, 73–81. https://doi.org/10.1111/j.1574-6976.2002.tb00599.x

Brown, M.E., Barros, T., Chang, M.C., 2012. Identification and characterization of a multifunctional dye peroxidase from a lignin-reactive bacterium. ACS Chem Biol 7, 2074–2081. https://doi.org/10.1021/cb300383y

Bugg, T.D., Rahmanpour, R., 2015. Enzymatic conversion of lignin into renewable chemicals. Curr Opin Chem Biol 29, 10–17. https://doi.org/10.1016/j.cbpa.2015.06.009

Buranov, A.U., Mazza, G., 2008. Lignin in straw of herbaceous crops. Ind. Crops Prod. 28, 237–259. https://doi.org/10.1016/j.indcrop.2008.03.008

Case, D.A., Cheatham 3rd, T.E., Darden, T., Gohlke, H., Luo, R., Merz Jr, K.M., Onufriev, A., Simmerling, C., Wang, B., Woods, R.J., 2005. The Amber biomolecular simulation programs. J. Comput. Chem. 26, 1668–1688. https://doi.org/10.1002/jcc.20290

Chandra, R., Raj, A., Purohit, H.J., Kapley, A., 2007. Characterisation and optimisation of three potential aerobic bacterial strains for kraft lignin degradation from pulp paper waste. Chemosphere 67, 839–846. https://doi.org/10.1016/j.chemosphere.2006.10.011

Dashtban, M., Schraft, H., Syed, T.A., Qin, W., 2010. Fungal biodegradation and enzymatic modification of lignin. Int J Biochem Mol Biol 1, 36–50.

Degrassi, G., Okeke, B.C., Bruschi, C. V, Venturi, V., 1998. Purification and characterization of an acetyl xylan esterase from Bacillus pumilus. Appl Env. Microbiol 64, 789–792.

Degrassi, G., Polverino De Laureto, P., Bruschi, C. V, 1995. Purification and characterization of ferulate and p-coumarate decarboxylase from Bacillus pumilus. Appl Env. Microbiol 61, 326–332.

Dieryckx, C., Gaudin, V., Dupuy, J.W., Bonneu, M., Girard, V., Job, D., 2015. Beyond plant defense: insights on the potential of salicylic and methylsalicylic acid to contain growth of the phytopathogen Botrytis cinerea. Front Plant Sci 6, 859. https://doi.org/10.3389/fpls.2015.00859

Dimitriou, P.S., Denesyuk, A., Takahashi, S., Yamashita, S., Johnson, M.S., Nakayama, T., Denessiouk, K., 2017. Alpha/beta-hydrolases: A unique structural motif coordinates catalytic acid residue in 40 protein fold families. Proteins Struct. Funct. Bioinforma. 85, 1845–1855. https://doi.org/10.1002/prot.25338

Dimitriou, P.S., Denesyuk, A.I., Nakayama, T., Johnson, M.S., Denessiouk, K., 2019. Distinctive structural motifs co-ordinate the catalytic nucleophile and the residues of the oxyanion hole in the alpha/beta-hydrolase fold enzymes. Protein Sci. 28, 344–364. https://doi.org/10.1002/pro.3527

Dodson, E.J., Winn, M., Ralph, A., 1997. Collaborative Computational Project, number 4: providing programs for protein crystallography. Methods Enzym. 277, 620–633.

https://doi.org/10.1016/s0076-6879(97)77034-4
Du, H., Klessig, D.F., 1997. Identification of a Soluble, High-Affinity Salicylic Acid-Binding Protein in Tobacco. Plant Physiol 113, 1319–1327. https://doi.org/10.1104/pp.113.4.1319
Durner, J., Shah, J., Klessig, D.F., 1997. Salicylic acid and disease resistance in plants. Trends Plant Sci. 2, 266–274. https://doi.org/Doi 10.1016/S1360-1385(97)86349-2
Emsley, P., Cowtan, K., 2004. Coot: model-building tools for molecular graphics. Acta Crystallogr D Biol Crystallogr 60, 2126–2132. https://doi.org/10.1107/S0907444904019158
Faulds, C.B., Williamson, G., 1994. Purification and Characterization of a Ferulic Acid Esterase (Fae-Iii) from Aspergillus-Niger - Specificity for the Phenolic Moiety and Binding to Microcrystalline Cellulose. Microbiology-Sgm 140, 779–787. https://doi.org/Doi 10.1099/00221287-140-4-779
Forouhar, F., Yang, Y., Kumar, D., Chen, Y., Fridman, E., Park, S.W., Chiang, Y., Acton, T.B., Montelione, G.T., Pichersky, E., Klessig, D.F., Tong, L., 2005. Structural and biochemical studies identify tobacco SABP2 as a methyl salicylate esterase and implicate it in plant innate immunity. Proc Natl Acad Sci U S A 102, 1773–1778. https://doi.org/10.1073/pnas.0409227102
Frago, S., Nicholls, R.D., Strickland, M., Hughes, J., Williams, C., Garner, L., Surakhy, M., Maclean, R., Rezgui, D., Prince, S.N., Zaccheo, O.J., Ebner, D., Sanegre, S., Yu, S., Buffa, F.M., Crump, M.P., Hassan, A.B., 2016. Functional evolution of IGF2:IGF2R domain 11 binding generates novel structural interactions and a specific IGF2 antagonist. Proc Natl Acad Sci U S A 113, E2766-75. https://doi.org/10.1073/pnas.1513023113
Garcia, B.L., Ball, A.S., Rodriguez, J., Perez-Leblic, M.I., Arias, M.E., Copa-Patino, J.L., 1998. Production and characterization of ferulic acid esterase activity in crude extracts by Streptomyces avermitilis CECT 3339. Appl. Microbiol. Biotechnol. 50, 213–218. https://doi.org/DOI 10.1007/s002530051279
Granja-Travez, R.S., Wilkinson, R.C., Persinoti, G.F., Squina, F.M., Fülöp, V., Bugg, T.D.H., 2018. Structural and functional characterisation of multi-copper oxidase CueO from lignin-degrading bacterium Ochrobactrum sp. reveal its activity towards lignin model compounds and lignosulfonate. FEBS J. 285, 1684–1700. https://doi.org/10.1111/febs.14437
Hatakka, A., 1994. Lignin-Modifying Enzymes from Selected White-Rot Fungi - Production and Role in Lignin Degradation. Fems Microbiol. Rev. 13, 125–135. https://doi.org/DOI 10.1111/j.1574-6976.1994.tb00039.x
Holm, L., 2020. DALI and the persistence of protein shape. Protein Sci. 29, 128–140. https://doi.org/10.1002/pro.3749
Holmquist, M., 2000. Alpha/Beta-hydrolase fold enzymes: structures, functions and mechanisms. Curr Protein Pept Sci 1, 209–235.
Hong, S., Lee, C., Jang, S.H., 2012. Purification and properties of an extracellular esterase from a cold-adapted Pseudomonas mandelii. Biotechnol Lett 34, 1051–1055. https://doi.org/10.1007/s10529-012-0866-y
Hotelier, T., Renault, L., Cousin, X., Negre, V., Marchot, P., Chatonnet, A., 2004. ESTHER, the database of the α/β-hydrolase fold superfamily of proteins. Nucleic Acids Res. 32, D145–D147. https://doi.org/10.1093/nar/gkh141
Huynh, K., Partch, C.L., 2015. Analysis of protein stability and ligand interactions by thermal shift assay. Curr Protoc Protein Sci 79, 28 9 1–14. https://doi.org/10.1002/0471140864.ps2809s79
Jones, G., Willett, P., Glen, R.C., 1995. Molecular recognition of receptor sites using a

genetic algorithm with a description of desolvation. J. Mol. Biol. 245, 43–53. https://doi.org/https://doi.org/10.1016/S0022-2836(95)80037-9
Jones, G., Willett, P., Glen, R.C., Leach, A.R., Taylor, R., 1997. Development and validation of a genetic algorithm for flexible docking11Edited by F. E. Cohen. J. Mol. Biol. 267, 727–748. https://doi.org/https://doi.org/10.1006/jmbi.1996.0897
Kabsch, W., 2010. Xds. Acta Crystallogr D Biol Crystallogr 66, 125–132. https://doi.org/10.1107/S0907444909047337
Kim, A.-Y., Shahzad, R., Kang, S.-M., Khan, A.L., Lee, S., Park, Y.-G., Lee, W.-H., Lee, I.-J., 2017. Paenibacillus terrae AY-38 resistance against Botrytis cinerea in Solanum lycopersicum L. plants through defence hormones regulation. J. Plant Interact. 12, 244–253. https://doi.org/10.1080/17429145.2017.1319502
Koes, D.R., Baumgartner, M.P., Camacho, C.J., 2013. Lessons learned in empirical scoring with smina from the CSAR 2011 benchmarking exercise. J. Chem. Inf. Model. 53, 1893–1904. https://doi.org/10.1021/ci300604z
Kosugi, A., Murashima, K., Doi, R.H., 2002. Xylanase and acetyl xylan esterase activities of XynA, a key subunit of the Clostridium cellulovorans cellulosome for xylan degradation. Appl Env. Microbiol 68, 6399–6402. https://doi.org/10.1128/aem.68.12.6399-6402.2002
Krissinel, E., Henrick, K., 2007. Inference of Macromolecular Assemblies from Crystalline State. J. Mol. Biol. 372, 774–797. https://doi.org/https://doi.org/10.1016/j.jmb.2007.05.022
Krissinel, E., Henrick, K., 2004. Secondary-structure matching (SSM), a new tool for fast protein structure alignment in three dimensions. Acta Crystallogr. Sect. D 60, 2256–2268. https://doi.org/doi:10.1107/S0907444904026460
Kumar, D., Klessig, D.F., 2003. High-affinity salicylic acid-binding protein 2 is required for plant innate immunity and has salicylic acid-stimulated lipase activity. Proc Natl Acad Sci U S A 100, 16101–16106. https://doi.org/10.1073/pnas.0307162100
Kumar, S., Bansal, M., 1998. Geometrical and sequence characteristics of alpha-helices in globular proteins. Biophys J 75, 1935–1944. https://doi.org/10.1016/S0006-3495(98)77634-9
Langer, G., Cohen, S.X., Lamzin, V.S., Perrakis, A., 2008. Automated macromolecular model building for X-ray crystallography using ARP/wARP version 7. Nat Protoc 3, 1171–1179. https://doi.org/10.1038/nprot.2008.91
Lebeis, S.L., Paredes, S.H., Lundberg, D.S., Breakfield, N., Gehring, J., McDonald, M., Malfatti, S., Glavina del Rio, T., Jones, C.D., Tringe, S.G., Dangl, J.L., 2015. PLANT MICROBIOME. Salicylic acid modulates colonization of the root microbiome by specific bacterial taxa. Science (80-.). 349, 860–864. https://doi.org/10.1126/science.aaa8764
Long, F., Vagin, A.A., Young, P., Murshudov, G.N., 2008. BALBES: a molecular-replacement pipeline. Acta Crystallogr D Biol Crystallogr 64, 125–132. https://doi.org/10.1107/S0907444907050172
Majumdar, S., Lukk, T., Solbiati, J.O., Bauer, S., Nair, S.K., Cronan, J.E., Gerlt, J.A., 2014. Roles of small laccases from Streptomyces in lignin degradation. Biochemistry 53, 4047–4058. https://doi.org/10.1021/bi500285t
Manohar, M., Tian, M., Moreau, M., Park, S.W., Choi, H.W., Fei, Z., Friso, G., Asif, M., Manosalva, P., von Dahl, C.C., Shi, K., Ma, S., Dinesh-Kumar, S.P., O'Doherty, I., Schroeder, F.C., van Wijk, K.J., Klessig, D.F., 2014. Identification of multiple salicylic acid-binding proteins using two high throughput screens. Front Plant Sci 5, 777. https://doi.org/10.3389/fpls.2014.00777
Mathews, S.L., Grunden, A.M., Pawlak, J., 2016. Degradation of lignocellulose and lignin by

Paenibacillus glucanolyticus. Int. Biodeterior. Biodegradation 110, 79–86. https://doi.org/10.1016/j.ibiod.2016.02.012
Mendes, R., Garbeva, P., Raaijmakers, J.M., 2013. The rhizosphere microbiome: significance of plant beneficial, plant pathogenic, and human pathogenic microorganisms. Fems Microbiol. Rev. 37, 634–663. https://doi.org/10.1111/1574-6976.12028
Millar, R., Rahmanpour, R., Yuan, E.W.J., White, C., Bugg, T.D.H., 2017. Esterase EstK from Pseudomonas putida mt-2: An enantioselective acetylesterase with activity for deacetylation of xylan and poly(vinylacetate). Biotechnol Appl Biochem 64, 803–809. https://doi.org/10.1002/bab.1536
Montella, I.R., Schama, R., Valle, D., 2012. The classification of esterases: an important gene family involved in insecticide resistance - A review. MemÃ\textthreesuperiorrias do Inst. Oswaldo Cruz 107, 437–449.
Murshudov, G.N., Vagin, A.A., Dodson, E.J., 1997. Refinement of macromolecular structures by the maximum-likelihood method. Acta Crystallogr D Biol Crystallogr 53, 240–255. https://doi.org/10.1107/S0907444996012255
Nardini, M., Dijkstra, B.W., 1999. Alpha/beta hydrolase fold enzymes: the family keeps growing. Curr Opin Struct Biol 9, 732–737.
Nielsen, H., Engelbrecht, J., Brunak, S., von Heijne, G., 1997. Identification of prokaryotic and eukaryotic signal peptides and prediction of their cleavage sites. Protein Eng 10, 1–6. https://doi.org/10.1093/protein/10.1.1
Padhi, S.K., Fujii, R., Legatt, G.A., Fossum, S.L., Berchtold, R., Kazlauskas, R.J., 2010. Switching from an Esterase to a Hydroxynitrile Lyase Mechanism Requires Only Two Amino Acid Substitutions. Chem. Biol. 17, 863–871. https://doi.org/https://doi.org/10.1016/j.chembiol.2010.06.013
Rahmanpour, R., Rea, D., Jamshidi, S., Fulop, V., Bugg, T.D., 2016. Structure of Thermobifida fusca DyP-type peroxidase and activity towards Kraft lignin and lignin model compounds. Arch Biochem Biophys 594, 54–60. https://doi.org/10.1016/j.abb.2016.02.019
Rashid, G.M., Taylor, C.R., Liu, Y., Zhang, X., Rea, D., Fulop, V., Bugg, T.D., 2015. Identification of Manganese Superoxide Dismutase from Sphingobacterium sp. T2 as a Novel Bacterial Enzyme for Lignin Oxidation. ACS Chem Biol 10, 2286–2294. https://doi.org/10.1021/acschembio.5b00298
Rashid, G.M.M., Durán-Peña, M.J., Rahmanpour, R., Sapsford, D., Bugg, T.D.H., 2017. Delignification and enhanced gas release from soil containing lignocellulose by treatment with bacterial lignin degraders. J. Appl. Microbiol. 123, 159–171. https://doi.org/10.1111/jam.13470
Rauwerdink, A., Kazlauskas, R.J., 2015. How the Same Core Catalytic Machinery Catalyzes 17 Different Reactions: the Serine-Histidine-Aspartate Catalytic Triad of α/β-Hydrolase Fold Enzymes. ACS Catal. 5, 6153–6176. https://doi.org/10.1021/acscatal.5b01539
Raymer, G., Willard, J.M., Schottel, J.L., 1990. Cloning, sequencing, and regulation of expression of an extracellular esterase gene from the plant pathogen Streptomyces scabies. J Bacteriol 172, 7020–7026. https://doi.org/10.1128/jb.172.12.7020-7026.1990
Record, E., Asther, M., Sigoillot, C., Pages, S., Punt, P.J., Delattre, M., Haon, M., van den Hondel, C.A., Sigoillot, J.C., Lesage-Meessen, L., Asther, M., 2003. Overproduction of the Aspergillus niger feruloyl esterase for pulp bleaching application. Appl Microbiol Biotechnol 62, 349–355. https://doi.org/10.1007/s00253-003-1325-4
Rogers, G.M., Jackson, S.A., Shelver, G.D., Baecker, A.A.W., 1992. Anaerobic Degradation of Lignocellulosic Substrates by a 1,4-Beta-Xylanolytic Clostridium Species Novum. Int. Biodeterior. Biodegradation 29, 3–17. https://doi.org/Doi 10.1016/0964-8305(92)90003-7

Rosado, A.S., de Azevedo, F.S., da Cruz, D.W., van Elsas, J.D., Seldin, L., 1998. Phenotypic and genetic diversity of Paenibacillus azotofixans strains isolated from the rhizoplane or rhizosphere soil of different grasses. J. Appl. Microbiol. 84, 216–226.
Shao, W.L., Wiegel, J., 1995. Purification and Characterization of 2 Thermostable Acetyl Xylan Esterases from Thermoanaerobacterium Sp Strain-Jw/Sl-Ys485. Appl. Environ. Microbiol. 61, 729–733.
Slaymaker, D.H., Navarre, D.A., Clark, D., del Pozo, O., Martin, G.B., Klessig, D.F., 2002. The tobacco salicylic acid-binding protein 3 (SABP3) is the.chloroplast carbonic anhydrase, which exhibits antioxidant activity and plays a role in the hypersensitive defense response. Proc. Natl. Acad. Sci. U. S. A. 99, 11640–11645. https://doi.org/10.1073/pnas.182427699
Song, H.Y., Lim, H.K., Kim, D.R., Lee, K.I., Hwang, I.T., 2014. A new bi-modular endo-beta-1,4-xylanase KRICT PX-3 from whole genome sequence of Paenibacillus terrae HPL-003. Enzyme Microb. Technol. 54, 1–7. https://doi.org/10.1016/j.enzmictec.2013.09.002
Stourac, J., Vavra, O., Kokkonen, P., Filipovic, J., Pinto, G., Brezovsky, J., Damborsky, J., Bednar, D., 2019. Caver Web 1.0: identification of tunnels and channels in proteins and analysis of ligand transport. Nucleic Acids Res. 47, W414–W422. https://doi.org/10.1093/nar/gkz378
ten Have, R., Teunissen, P.J., 2001. Oxidative mechanisms involved in lignin degradation by white-rot fungi. Chem Rev 101, 3397–3413.
Till, M., Goldstone, D.C., Attwood, G.T., Moon, C.D., Kelly, W.J., Arcus, V.L., 2013. Structure and function of an acetyl xylan esterase (Est2A) from the rumen bacterium Butyrivibrio proteoclasticus. Proteins 81, 911–917. https://doi.org/10.1002/prot.24254
Timmusk, S., Paalme, V., Lagercrantz, U., Nevo, E., 2009. Detection and quantification of Paenibacillus polymyxa in the rhizosphere of wild barley (Hordeum spontaneum) with real-time PCR. J. Appl. Microbiol. 107, 736–745. https://doi.org/10.1111/j.1365-2672.2009.04265.x
Topakas, E., Vafiadi, C., Christakopoulos, P., 2007. Microbial production, characterization and applications of feruloyl esterases. Process Biochem. 42, 497–509. https://doi.org/10.1016/j.procbio.2007.01.007
Tripathi, D., Jiang, Y.L., Kumar, D., 2010. SABP2, a methyl salicylate esterase is required for the systemic acquired resistance induced by acibenzolar-S-methyl in plants. FEBS Lett 584, 3458–3463. https://doi.org/10.1016/j.febslet.2010.06.046
Uhlik, O., Jecna, K., Mackova, M., Vlcek, C., Hroudova, M., Demnerova, K., Paces, V., Macek, T., 2009. Biphenyl-metabolizing bacteria in the rhizosphere of horseradish and bulk soil contaminated by polychlorinated biphenyls as revealed by stable isotope probing. Appl Env. Microbiol 75, 6471–6477. https://doi.org/10.1128/AEM.00466-09
van Pouderoyen, G., Eggert, T., Jaeger, K.E., Dijkstra, B.W., 2001. The crystal structure of Bacillus subtilis lipase: a minimal alpha/beta hydrolase fold enzyme. J Mol Biol 309, 215–226. https://doi.org/10.1006/jmbi.2001.4659
Veach, A.M., Morris, R., Yip, D.Z., Yang, Z.K., Engle, N.L., Cregger, M.A., Tschaplinski, T.J., Schadt, C.W., 2019. Rhizosphere microbiomes diverge among Populus trichocarpa plant-host genotypes and chemotypes, but it depends on soil origin. Microbiome 7, 76. https://doi.org/10.1186/s40168-019-0668-8
Vivoli, M., Novak, H.R., Littlechild, J.A., Harmer, N.J., 2014. Determination of protein-ligand interactions using differential scanning fluorimetry. J Vis Exp 51809. https://doi.org/10.3791/51809
Vlot, A.C., Liu, P.-P., Cameron, R.K., Park, S.-W., Yang, Y., Kumar, D., Zhou, F., Padukkavidana, T., Gustafsson, C., Pichersky, E., Klessig, D.F., 2008. Identification of

likely orthologs of tobacco salicylic acid-binding protein 2 and their role in systemic acquired resistance in Arabidopsis thaliana. Plant J. 56, 445–456. https://doi.org/10.1111/j.1365-313X.2008.03618.x

Wang, Y.X., Liu, Q., Yan, L., Gao, Y.M., Wang, Y.J., Wang, W.D., 2013. A novel lignin degradation bacterial consortium for efficient pulping. Bioresour. Technol. 139, 113–119. https://doi.org/10.1016/j.biortech.2013.04.033

Watanabe, M., Fukada, H., Inoue, H., Ishikawa, K., 2015. Crystal structure of an acetylesterase from Talaromyces cellulolyticus and the importance of a disulfide bond near the active site. FEBS Lett. 589, 1200–1206. https://doi.org/10.1016/j.febslet.2015.03.020

Wong, D.W.S., 2006. Feruloyl esterase - A key enzyme in biomass degradation. Appl. Biochem. Biotechnol. 133, 87–112. https://doi.org/Doi 10.1385/Abab:133:2:87

Zakzeski, J., Bruijnincx, P.C., Jongerius, A.L., Weckhuysen, B.M., 2010. The catalytic valorization of lignin for the production of renewable chemicals. Chem Rev 110, 3552–3599. https://doi.org/10.1021/cr900354u

Zhao, N., Guan, J., Forouhar, F., Tschaplinski, T.J., Cheng, Z.-M., Tong, L., Chen, F., 2009. Two poplar methyl salicylate esterases display comparable biochemical properties but divergent expression patterns. Phytochemistry 70, 32–39. https://doi.org/https://doi.org/10.1016/j.phytochem.2008.11.014